

# An unknown branch of the total-transmission modes for the Kerr-geometry

Gregory B. Cook,\* Luke S. Annichiarico,† and Daniel J. Vickers‡

*Department of Physics, Wake Forest University, Winston-Salem, North Carolina 27109*

(Dated: January 11, 2019)

The gravitational modes of the Kerr geometry include both quasinormal modes and total-transmission modes. Sequences of these modes are parameterized by the angular momentum of the black hole. The quasinormal and total-transmission modes are usually distinct, having mode frequencies that are different at any given value of the angular momentum. But a discrete and countably infinite subset of the left-total-transmission modes are simultaneously quasinormal modes. Most of these special modes exist along previously unknown branches of the gravitational total-transmission modes. In this paper, we give detailed plots of the total-transmission modes for harmonic indices  $\ell = [2, 7]$ , with special emphasis given to the  $m = 0$  modes which all contain previously unknown branches. All of these unknown branches have purely imaginary mode frequencies. We find that as we approach the Schwarzschild limit along these new branches, the mode frequencies approach  $-i\infty$  in stark contrast to the finite mode frequency obtained in the Schwarzschild limit along the previously known branches. We explain when and why, at certain frequencies, the left-total-transmission modes are simultaneously quasinormal modes. At these same frequencies, the right-total-transmission modes are missing. We also derive analytic expressions for the asymptotic behavior of the total-transmission mode frequencies, and for the values of the angular momentum at which the modes are simultaneously quasinormal modes.

PACS numbers: 04.20.-q, 04.70.Bw, 04.20.Cv, 04.30.Nk

## I. INTRODUCTION

The Kerr geometry[1] is one of the most astrophysically important solutions of Einstein's equations. It represents an isolated black hole with angular momentum, and the linear perturbations of the Kerr geometry are used to understand the late-time behavior of astrophysical events, such as the merger of compact objects, that results in a black hole. In particular, the quasinormal modes (QNMs) of the Kerr spacetime are used to model the ring-down portion of a gravitational waveform, for example from a binary-black-hole merger[2–5].

The gravitational modes of the Kerr geometry include not only the QNMs, but also the total transmission modes (TTMs). The QNMs are defined by their allowing no disturbances to enter the system from either infinity or from the black-hole boundary. There are two types of TTMs, each changing one of the conditions used in defining QNMs. Left TTMs ( $\text{TTM}_{\text{LS}}$ ) switch the boundary condition at the black-hole boundary. Essentially,  $\text{TTM}_{\text{LS}}$  represent disturbances that can move from the vicinity of the black hole toward spatial infinity without reflections that would propagate into the black hole. Right TTMs ( $\text{TTM}_{\text{RS}}$ ) switch the boundary condition at spatial infinity. Essentially,  $\text{TTM}_{\text{RS}}$  represent disturbances that can move from spatial infinity toward the black hole without reflections that would propagate back toward spatial infinity. Switching both boundary conditions would represent a bound state which does not exist

for perturbations of the Kerr geometry. In this paper, we will be primarily interested in the gravitational TTMs of the Kerr geometry.

The TTMs were first explored, in the context of algebraically special modes, by Wald[6] and in more detail by Chandrasekhar[7]. In the Schwarzschild limit, the TTMs and their complex frequencies  $\omega$  can be determined analytically. In general, the mode frequencies,  $\omega$ , are functions of the angular momentum of the black hole, and must be determined numerically. The modes and their frequencies are conveniently parameterized by the dimensionless angular momentum  $\bar{a} = a/M$ , where  $M$  is the mass of the black hole, and  $J = aM$  is the angular momentum. In the Schwarzschild limit,  $\bar{a} = 0$ , the TTM frequencies  $\omega(\bar{a})$  become

$$M\omega(0) \equiv \bar{\Omega}_\ell \equiv -\frac{i}{12}(\ell-1)\ell(\ell+1)(\ell+2), \quad (1)$$

which are purely imaginary. In general the mode frequencies  $\omega(\bar{a})$  are complex and the  $\text{TTM}_{\text{LS}}$  and  $\text{TTM}_{\text{RS}}$  share the same set of mode frequencies, although the modes themselves differ.

The first numerical results for the mode frequencies of the TTMs were included in Chandrasekhar's derivation of these algebraically special perturbations[7]. There, a few values were given for each of the five modes for  $\ell = 2$ . More detailed plots for the  $\ell = 2$  modes were shown by Onozawa[8]. More recently, one of us reported the mode frequencies for both  $\ell = 2$  and  $\ell = 3$ [9]. Interestingly, numerical investigations[8, 10] showed that in the Schwarzschild limit, certain QNM frequencies also approached the same set of purely imaginary mode frequencies  $\bar{\Omega}_\ell$ . There was considerable confusion about the nature of the modes with these frequencies, but this confusion was set to rest by Massen van den Brink[11]. He

\* cookgb@wfu.edu

† annils14@wfu.edu

‡ vickdj14@wfu.edu

showed that the  $\text{TMM}_L$  associated with a given  $\bar{\Omega}_\ell$  was actually, simultaneously a QNM. At the same time, the corresponding solution thought to be a  $\text{TMM}_R$  was neither a TTM nor a QNM. These conclusions are based on a careful examination of the behavior of the modes at the black-hole horizon (see Refs. [11] or [12] for more detail.)

Recent high-precision explorations of the gravitational QNMs of the Kerr geometry found a large number of additional cases where sequences of QNM frequencies  $\omega(\bar{a})$  approached the negative imaginary axis (NIA) for values of  $\bar{a} \neq 0$ [12]. The nature of the modes associated with these new, purely imaginary mode frequencies was explored[12, 13] using the theory of Heun polynomials[14], expanding on the previous work by Massen van den Brink[11].

In certain cases, the sequence of QNMs could have frequencies approach the NIA, but could not exist with  $\omega(\bar{a})$  precisely on the NIA. In other cases, all with  $m = 0$ , the sequence of QNMs could extend to have  $\omega(\bar{a})$  on the NIA. In this case, two possible behaviors were seen. Either the mode was simply a QNM, or it was simultaneously a QNM and a  $\text{TMM}_L$ . This latter case is an extension of the behavior seen in the Schwarzschild limit (ie. the modes with frequencies  $\bar{\Omega}_\ell$ .)

Let us reconsider this with emphasis on the behavior of the TTMs. For generic values of  $\bar{a}$ , the  $\text{TMM}_L$ s and  $\text{TMM}_R$ s share the same set of mode frequencies. In the Schwarzschild limit,  $\bar{a} = 0$ , the various  $m$  modes are degenerate. Also, the  $\text{TMM}_L$ s are simultaneously QNMs while the solutions that should be  $\text{TMM}_R$ s are missing. It was seen in Ref. [12] that for certain values of  $\bar{a} > 0$  for  $\ell = 2-4$  and  $m = 0$ , certain QNMs on the NIA were also simultaneously  $\text{TMM}_L$ s. At these same values of  $\bar{a}$ , the corresponding  $\text{TMM}_R$ s did not exist. This behavior occurred at certain points along  $m = 0$  TTM sequences within the range  $0 \leq \bar{a} < \bar{a}_{\text{crit}}$  (where  $\bar{a}_{\text{crit}}$  is a function of  $\ell$ ), and within this range  $\omega(\bar{a})$  is purely imaginary. For  $\bar{a}_{\text{crit}} < \bar{a} \leq 1$ , the  $m = 0$  TTM sequences of mode frequencies move off of the NIA, obtaining general complex values.

However, we found[12] that for each  $\ell = 2-4$  and  $m = 0$ , there are a seemingly countably infinite number of QNMs with  $\bar{a} < \bar{a}_{\text{crit}}$  that are also simultaneously  $\text{TMM}_L$ s (and at which the  $\text{TMM}_R$ s do not exist), but which do not correspond to known segments of the TTM sequences. This indicated that a previously unknown branch exists for each of the  $m = 0$  TTM sequences. In this paper, we verify this conjecture by explicitly computing these sequences for  $\ell = 2-7$ .

Interestingly, the mode frequencies of this new branch of the  $m = 0$  TTMs approach  $-i\infty$  as  $\bar{a} \rightarrow 0$ . We find that it is possible to construct an analytic expression for the asymptotic behavior of these branches. Doing so required that we find an analytic expression for the separation constant  ${}_sA_{\ell m}(c)$  of the spin-weighted spheroidal harmonics in the asymptotic prolate case (large purely imaginary  $c$ ) for  $m = 0$ . To our knowledge this has been known only to leading order for  $s = \pm 2$ .

This paper proceeds as follows. In Sec. II, we will briefly review the methods used to construct TTMs of the Kerr geometry. In Sec. III, we will examine numerical results for the TTMs. In Sec. IV, we will find an asymptotic expansion for both the mode frequencies,  $\omega(\bar{a})$  of the TTMs and for the separation constant  ${}_sA_{\ell m}(c)$  of the spin-weighted spheroidal harmonics. Finally, in Sec. V, we will review the prior results from Ref.[12] that describe where along the TTM sequences the modes change their behavior, and end with some final discussion.

## II. METHODS

Modes of the Kerr geometry can be obtained by solving the Teukolsky master equation with appropriate boundary conditions. Our approach for obtaining the QNMs of the Kerr geometry is outlined in detail in Refs. [9] and [12]. Our methods for obtaining the TTMs are essentially the same, but with a few necessary differences.

In vacuum, the Teukolsky master equation separates using

$${}_s\psi(t, r, \theta, \phi) = e^{-i\omega t} e^{im\phi} S(\theta)R(r). \quad (2)$$

The radial function  $R(r)$  then satisfies the radial Teukolsky equation

$$\Delta^{-s} \frac{d}{dr} \left[ \Delta^{s+1} \frac{dR(r)}{dr} \right] + \left[ \frac{K^2 - 2is(r-M)K}{\Delta} + 4is\omega r - \lambda \right] R(r) = 0, \quad (3a)$$

where

$$\Delta \equiv r^2 - 2Mr + a^2, \quad (3b)$$

$$K \equiv (r^2 + a^2)\omega - am, \quad (3c)$$

$$\lambda \equiv {}_sA_{\ell m}(a\omega) + a^2\omega^2 - 2am\omega, \quad (3d)$$

and Boyer-Lindquist coordinates are used.  ${}_sA_{\ell m}(a\omega)$  is the angular separation constant associated with the angular Teukolsky equation governing  $S(\theta)$ . With  $x = \cos\theta$ , the function  $S(\theta) = {}_sS_{\ell m}(x; a\omega)$  is the spin-weighted spheroidal function satisfying

$$\partial_x \left[ (1-x^2) \partial_x [{}_sS_{\ell m}(x; c)] \right] + \left[ (cx)^2 - 2csx + s + {}_sA_{\ell m}(c) - \frac{(m+sx)^2}{1-x^2} \right] {}_sS_{\ell m}(x; c) = 0, \quad (4)$$

where  $c (= a\omega)$  is the oblateness parameter and  $m$  the azimuthal separation constant. Finally,  $\ell$  is the harmonic mode index which labels the elements in the set of eigen-solutions of the angular equation for fixed values of  $s, m$ , and  $c$ .

Both Eqs. (3a) and (4) are examples of the general class of confluent Heun equations. We have found it particularly useful to work with the radial equation, Eq. (3a), within the context of confluent Heun theory[14]. Following Borissov and Fiziev[15], the radial equation can be written in the nonsymmetrical canonical form of the confluent Heun equation in 8 different ways, depending on the choice of three parameters. Following Ref. [9], we denote these three parameters as  $\bar{\zeta}$ ,  $\xi$ , and  $\eta$ . Each parameter has two possible choices:

$$\bar{\zeta} = \bar{\zeta}_{\pm}, \quad \xi = \xi_{\pm}, \quad \text{and} \quad \eta = \eta_{\pm}. \quad (5)$$

These three parameters are associated with the regular behavior of solutions of the confluent Heun equation at the three singular points. See Ref. [9] for details. Regular singular points occur at the Cauchy and event horizons, with the choice of  $\xi$  fixing the behavior at the event horizon, and  $\eta$  fixing the behavior at the Cauchy horizon. The singular point at infinity is irregular, and is fixed by the choice of  $\bar{\zeta}$ . See Sec. II.C of Ref. [9] for details.

There are two local Frobenius solutions at each singular point, but more interesting are the solutions known as *confluent Heun functions* and *confluent Heun polynomials*. Confluent Heun functions are solutions that are simultaneously Frobenius solutions at two adjacent singular points. For our purposes, they arise when we fix boundary conditions at two singular points and find values of some parameter that allows both boundary conditions to be satisfied. In general, confluent Heun functions are infinite-series solutions. Confluent Heun polynomials are an important subset of the confluent Heun functions where the solutions are simultaneously Frobenius solutions of all three singular points. In this case, the infinite-series solutions truncate to yield a polynomial solution.

By making an additional coordinate transformation and an appropriate redefinition of the solution function (see Sec. II.C.1 of Ref. [9] for details), the resulting equation takes a form where the only solution that is finite at both singular points is the solution that satisfies the desired boundary conditions. In this form, the desired confluent Heun functions can be found using Leaver's continued-fraction approach[10]. As outlined in Sec. IV.B of Ref.[12], the choices  $\bar{\zeta} = \bar{\zeta}_+$  and  $\xi = \xi_-$  (see Eqns. (19a) and (19b) in [12]) together with a specific redefinition of the solution function allows the continued-fraction method to find confluent Heun functions which are QNMs. The entire procedure is extensible to finding TTMs by simply changing the choice of  $\xi$  to  $\xi_+$ , in which case the confluent Heun functions are TTM<sub>L</sub>s. To find TTM<sub>RS</sub>, we instead change the choice of  $\bar{\zeta}$  to  $\bar{\zeta}_-$ .

In more detail, the continued-fraction solution of Eq. (30) in Ref. [9] is unchanged except for how the choices for the  $\xi$  and  $\bar{\zeta}$  parameters affect the evaluation of the coefficients in Eqs. (31a-e) and (38a-c) of [9]. The only changes in the discussion of the existence of minimal solutions of the continued fraction found in Ref. [12] come from the fact that for TTM<sub>RS</sub>, the branch cut of

$u_1(\bar{\omega})$  (see discussion below Eq. (25b)) is along the positive imaginary axis, which means that  $\text{Re}(u_1(\bar{\omega})) \neq 0$  on the NIA. This means that the continued fraction can be used to determine the TTM<sub>R</sub> frequencies on the NIA, in contrast with the QNM and TTM<sub>L</sub> cases.

In addition to the confluent Heun function mode solutions of the Teukolsky radial equation, there also exist confluent Heun polynomial mode solutions. For TTMs, the derivation of the polynomial modes can be found in Sec. III.B of Ref.[9]. There, we find that the condition for the existence of confluent Heun polynomial solutions is equivalent to the vanishing of the magnitude squared of the Starobinsky constant[6, 7]. We write the magnitude squared of the Starobinsky constant as

$$|Q|^2 = \lambda^2(\lambda + 2)^2 + 8\lambda\bar{a}\bar{\omega}(6(\bar{a}\bar{\omega} + m) - 5\lambda(\bar{a}\bar{\omega} - m)) + 144\bar{\omega}^2(1 + \bar{a}^2(\bar{a}\bar{\omega} - m)^2), \quad (6)$$

where  $\bar{\omega} \equiv M\omega$  is the dimensionless mode frequency. For TTM<sub>L</sub>s, take  $s = -2$  and

$$\lambda = \lambda_- \equiv {}_{-2}A_{\ell m}(\bar{a}\bar{\omega}) + \bar{a}^2\bar{\omega}^2 - 2m\bar{a}\bar{\omega}. \quad (7)$$

For TTM<sub>RS</sub>, take  $s = +2$  and

$$\lambda = \lambda_+ \equiv {}_2A_{\ell m}(\bar{a}\bar{\omega}) + \bar{a}^2\bar{\omega}^2 - 2m\bar{a}\bar{\omega} + 4. \quad (8)$$

However, because  ${}_{-s}A_{\ell m}(\bar{a}\bar{\omega}) = {}_sA_{\ell m}(\bar{a}\bar{\omega}) + 2s$ , it follows that  $\lambda_+ = \lambda_-$  and we find that the TTM<sub>L</sub> and TTM<sub>R</sub> algebraically special modes will share the same frequency spectrum. For  $\bar{a} > 0$ , numerical values for the TTM mode frequencies  $\bar{\omega}$  are obtained by finding roots of Eq. (6) where values for  ${}_sA_{\ell m}(\bar{a}\bar{\omega})$  are obtained by solving the angular Teukolsky equation, Eq. (4), using the spectral solver described in Sec. II.D.1 of Ref.[9].

For QNMs, the derivation of the polynomial modes can be found in Sec. IV.C of Ref. [12]. Confluent Heun polynomial QNM solutions can exist in two classes distinguished by the choice of the  $\eta$  parameter. For both classes, there is a necessary, but not sufficient condition placed on the value of  $\bar{\omega}$  in order for a polynomial QNM solution to exist. A corresponding constraint on the TTM frequencies does not exist. The constraints on the values of  $\bar{\omega}$  for polynomial QNM solutions can be written as

$$\bar{\omega} = \bar{\omega}_+ \equiv \frac{\bar{a}m - iN_+\sqrt{1 - \bar{a}^2}}{2(1 + \sqrt{1 - \bar{a}^2})}, \quad (9)$$

or

$$\bar{\omega} = \bar{\omega}_- \equiv -i\frac{N_-}{4}, \quad (10)$$

where  $N_+ \geq s+1$  and  $N_- \geq 1$  take on integer values. The necessary and sufficient condition for a polynomial QNM solution to exist is referred to as the  $\Delta_{q+1} = 0$  condition, and is described in detail in Sec. IV.C.1 of Ref. [12]. The vanishing of the magnitude squared of the Starobinsky constant is a special case of the  $\Delta_{q+1} = 0$  condition.

As discussed in Sec. IV.D of Ref. [12], for potential QNM polynomial modes, we must pay particular attention to the behavior of the solution at the event horizon. The constraint that  $\bar{\omega} = \bar{\omega}_+$  is precisely the condition that the roots of the indicial equation differ by an integer for local Frobenius solutions at the event horizon. Summarizing the results of Ref. [12], all of the potential polynomial QNM modes found have  $m = 0$ . The majority of potential QNM modes satisfying  $\bar{\omega} = \bar{\omega}_+$  are *miraculous*. That is, such a mode is neither QNM nor  $\text{TMM}_L$ <sup>1</sup>. However, a subset of potential QNM modes are *anomalous*. That is, such a mode is simultaneously a QNM and a  $\text{TMM}_L$ . In fact, these anomalous QNM solutions also satisfy the condition  $|\mathcal{Q}|^2 = 0$  for polynomial  $\text{TMM}_L$ s. Finally, while not of direct interest to the remainder of this paper, all of the potential QNM modes satisfying  $\bar{\omega} = \bar{\omega}_-$  have proven to be generic. That is, the roots of the indicial equation do not differ by an integer, and the solutions are simply QNMs.

### III. NUMERICAL RESULTS.

The first numerical results for the mode frequencies of the TTMs were included in Chandrasekhar's derivation of these algebraically special perturbations[7]. There, a few values were given for each of the five modes for  $\ell = 2$ . More detailed plots for the  $\ell = 2$  modes were shown by Onozawa[8]. More recently, we reported the mode frequencies for both  $\ell = 2$  and  $\ell = 3$ [9]. Figure 1 shows the various  $\ell = 2$  TTM mode frequency sequences. All start at the Schwarzschild limit at the point  $\bar{\omega} = -2i$ . The  $m = 1$  and  $m = 2$  sequences extend rightward from this point. The  $m = 0$  sequence first extends up the NIA. This portion of the sequence is labeled  $m = 0_0$  in the figure, and covers the range  $0 \leq \bar{a} \lesssim 0.494445955$ . For  $0.494445955 \lesssim \bar{a} \leq 1$ , the  $m = 0$  sequence abruptly turns off of the NIA and extends rightward. This segment of the sequence is labeled  $m = 0_1$  in the figure. The segment of the sequence labeled  $m = 0_2$  is the previously unknown segment of the sequence first noticed in Ref. [12]. It also covers the range  $0 \leq \bar{a} \lesssim 0.494445955$  covered by the  $m = 0_0$  segment, but  $\lim_{\bar{a} \rightarrow 0} \bar{\omega} = -i\infty$ .

The behavior of the  $\ell = 2$ ,  $m = 0$  sequence can be more fully understood by plotting the real and imaginary parts of  $\bar{\omega}$  separately as functions of  $\bar{a}$ . Figure 2 shows the 3 different  $m = 0$  segments as functions of  $\bar{a}$ . Note that for the  $\text{Im}(\bar{\omega})$ , the  $m = 0_0$  segment continues smoothly into the  $m = 0_2$  segment at the critical value of  $\bar{a}$  (where  $d\bar{\omega}/d\bar{a} = \infty$ ), while the  $m = 0_1$  segment emerges discontinuously from this point.

The behavior for  $\ell > 2$  is similar. Figures 3– 7 show sequences of the complex frequency  $\bar{\omega}$  for all TTMs for

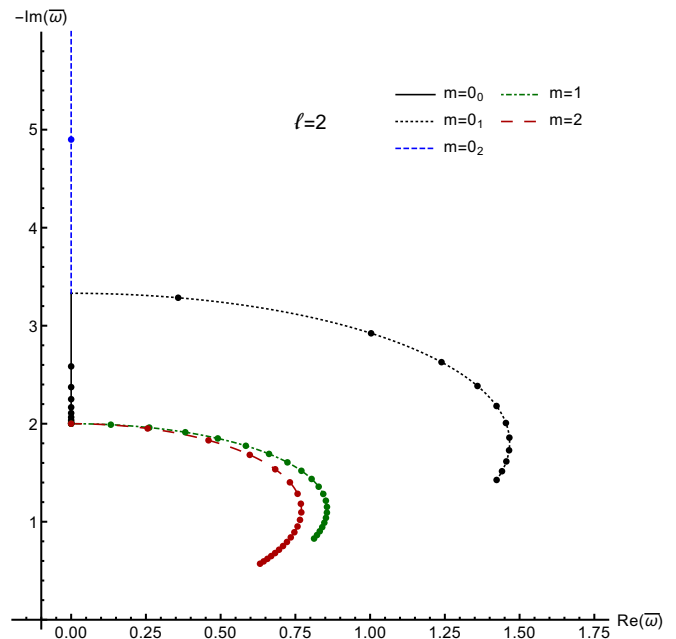


FIG. 1. The complex frequency  $\bar{\omega}$  is plotted for the Kerr TTM  $\ell = 2$  modes. Note that the imaginary axis is inverted. Each sequence covers the range  $0 \leq \bar{a} \leq 1$ , with markers on each sequence denoting a change in  $\bar{a}$  of 0.05. The sequences labeled  $m = 0_0$  and  $0_1$  are the previously known segments of the  $m = 0$  sequence. The segment labeled  $m = 0_2$  is the previously unknown branch of the  $m = 0$  sequence.

$\ell = 3$ –7, and the  $\text{Im}(\bar{\omega})$  as a function of  $\bar{a}$  for each  $m = 0$  mode sequence.

From fundamental symmetries of the radial and angular Teukolsky equations, it is well known that mode frequencies come in pairs related by

$$\omega_{\ell-m}(a) = -\omega_{\ell m}^*(a). \quad (11)$$

For QNMs, there are two complete sets of modes. That is, for given  $\ell$ , there are  $2\ell + 1$  mode frequencies with  $\text{Re}(\omega) > 0$ , and a complementary set with  $\text{Re}(\omega) < 0$  that are related by Eq. (11). As made clear by Berti *et al*[16], the existence of a second set of modes satisfying the symmetry of Eq. (11) is necessary to asymptotically represent both polarizations of gravitational waves in terms of QNMs.

The situation is somewhat different for the TTMs. There are no TTMs where the  $\text{Re}(\bar{\omega}) > 0$  and  $m < 0$ . There are TTMs with  $m < 0$ , but these all have  $\text{Re}(\bar{\omega}) < 0$ . They are solutions from the complementary set of modes satisfying Eq. (11). The  $m = 0$  modes also obey this relationship, so there are a pair of  $m = 0$  solutions, the  $m = 0_0$  and  $0_2$  segments are degenerate with their complementary counterparts, but the  $\text{Re}(\bar{\omega})$  of the  $m = 0_1$  segments have opposite signs.

Including the  $m = 0$  case, these *known* polynomial modes have only  $\ell + 1$  values of  $m$  in each of these complementary sets, rather than the expected  $2\ell + 1$  values of  $m$ . Is it possible that the remaining  $\ell$  values of

<sup>1</sup> It cannot be  $\text{TMM}_R$  because of the boundary condition at infinity.

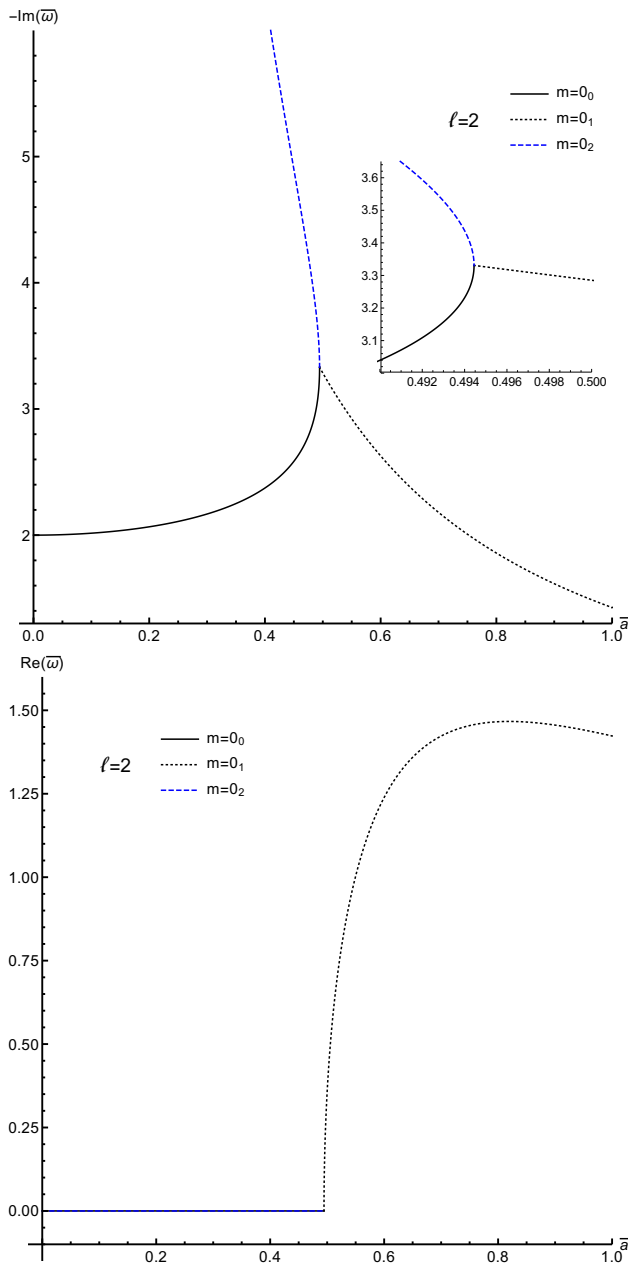


FIG. 2. The real and imaginary parts of the complex frequency  $\bar{\omega}$  is plotted as a function of  $\bar{a}$  for the Kerr TTM  $\ell = 2$ ,  $m = 0$  sequence. Note that the axis is inverted for the  $\text{Im}(\bar{\omega})$ . For the  $\text{Im}(\bar{\omega})$ , the  $m = 0_2$  segment continues towards  $-i\infty$  and asymptotes to the NIA. The inset in the first plot shows the behavior near the critical value of  $\bar{a}$ . For the  $\text{Re}(\bar{\omega})$ , the  $m = 0_0$  and  $0_2$  segments overlap with  $\text{Re}(\bar{\omega}) = 0$  along these segments.

$m$  that we might expect to find are actually confluent-Heun functions (general infinite-series solutions) rather than polynomials? As mentioned in Sec. II, the condition for the existence of polynomial solutions is equivalent to the vanishing of the magnitude squared of the Starobinsky constant, so the polynomial solutions are both algebraically special and TTMs. Both Wald[6] and

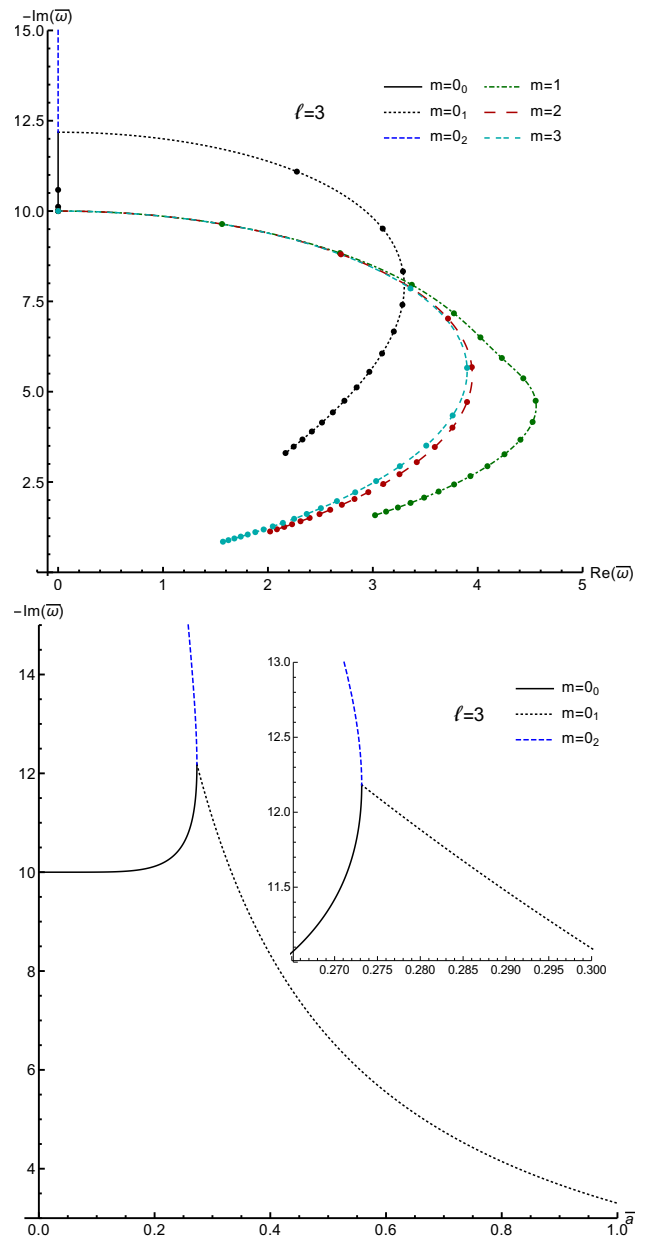


FIG. 3. The first plot shows the complex frequency  $\bar{\omega}$  for all of the TTM  $\ell = 3$  sequences. The second plot shows the  $\text{Im}(\bar{\omega})$  as a function of  $\bar{a}$  for the Kerr TTM  $\ell = 3$ ,  $m = 0$  sequence. Note that the  $\text{Im}(\bar{\omega})$  axis is inverted for both plots. The inset in the second plot shows the behavior near the critical value of  $\bar{a}$ . The  $\text{Im}(\bar{\omega})$  for the  $m = 0_2$  segment continues towards  $-i\infty$  and asymptotes to the NIA.

Chandrasekhar[7] have shown that the vanishing of the Starobinsky constant is the necessary and sufficient conditions for algebraically-special solutions. If all TTMs are algebraically special, then there can be no TTMs in the form of confluent-Heun functions. While it seems that the algebraically-special solutions should encompass all of the TTMs, we would like to verify that some subtlety associated with the inner boundary condition doesn't al-

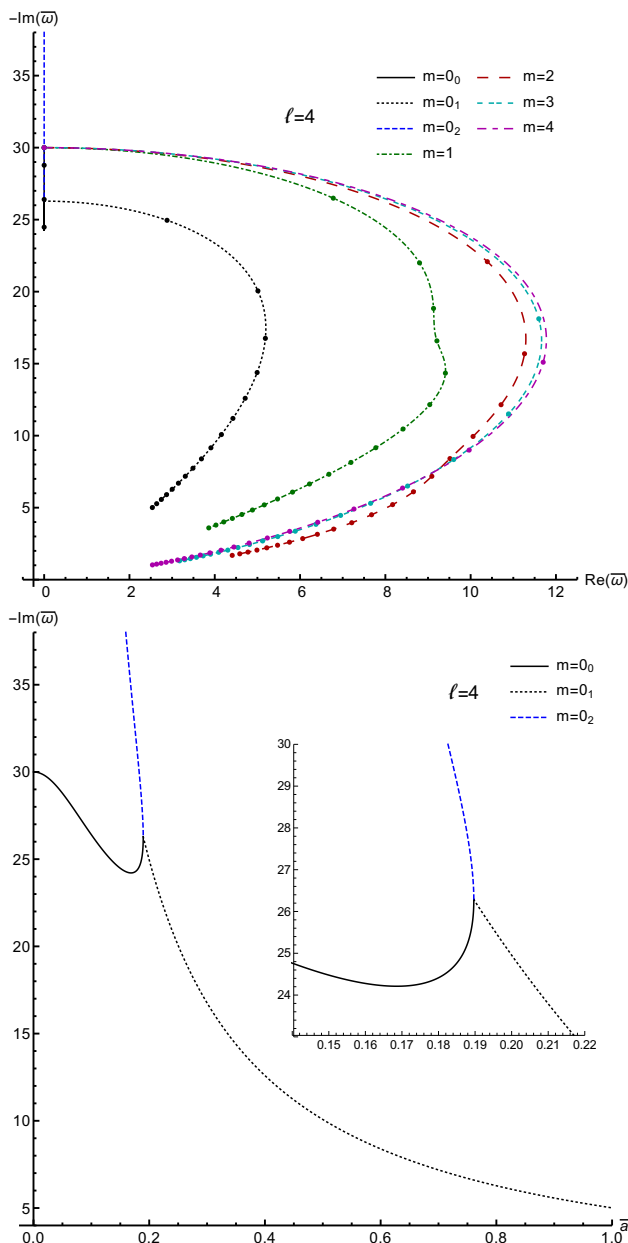


FIG. 4. The TTMs for  $\ell = 4$ . See the caption to Fig. 3 for details.

low for the existence of confluent-Heun function TTMs. We can do this by explicitly searching for them, and have done so. An extensive search for confluent-Heun function solutions for the TTMs<sup>2</sup> found no evidence for any

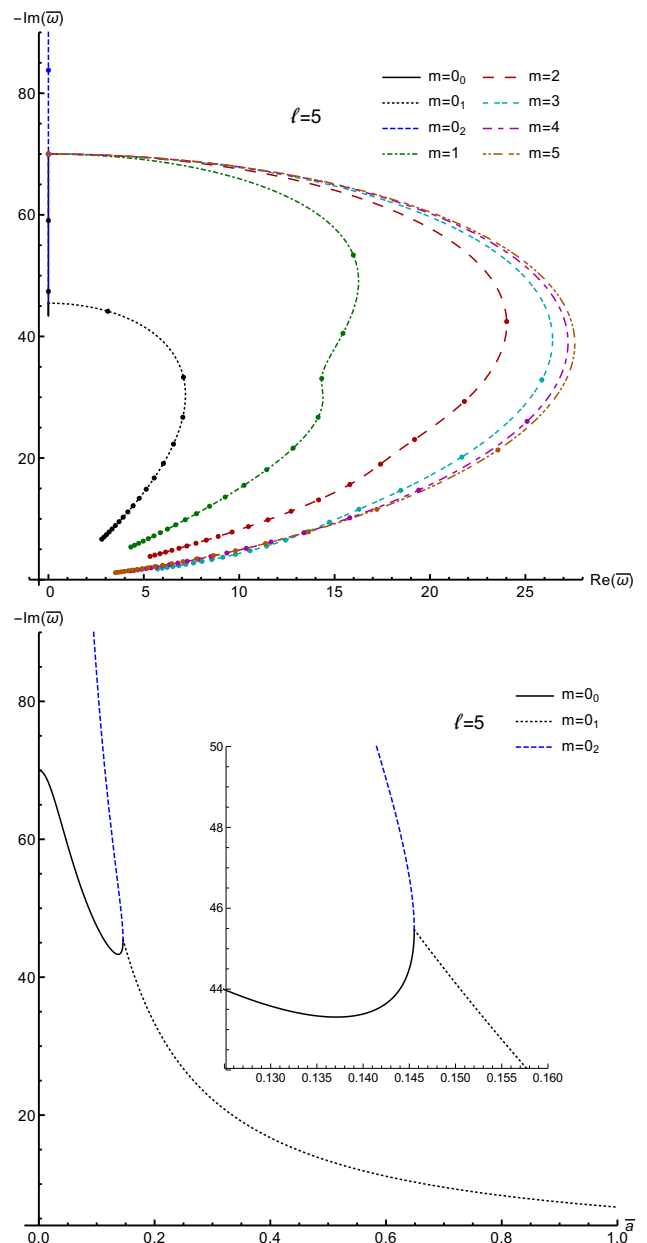


FIG. 5. The TTMs for  $\ell = 5$ . See the caption to Fig. 3 for details.

<sup>2</sup> To search for TTMs that are confluent-Heun functions, we examined contour plots of the real and imaginary parts of the continued fraction function whose roots designate the TTMs. We examined the first 3  $\ell$  values for  $m = 0, \pm 1, \pm 2$ , and  $\pm 3$ . For each case, we considered  $\bar{a} = 0.2, 0.4, 0.6$ , and  $0.8$ . Finally, we looked for roots in the range  $-5 \leq \text{Re}(\bar{\omega}) \leq 25$  and  $-30 \leq \text{Im}(\bar{\omega}) \leq 0$ . All candidate roots were further examined and found to be polynomial modes.

such solutions. *Interestingly, we did find previously unknown polynomial TTM (algebraically-special) solutions, all of which start at complex infinity in the limit that  $\bar{a} \rightarrow 0$ .* These new solutions were discovered after this paper was submitted, while we were verifying the absence of confluent-Heun function TTMs using the more methodical search described in footnote 2. We are currently exploring the details of these new TTMs, and will report on them in a future paper.

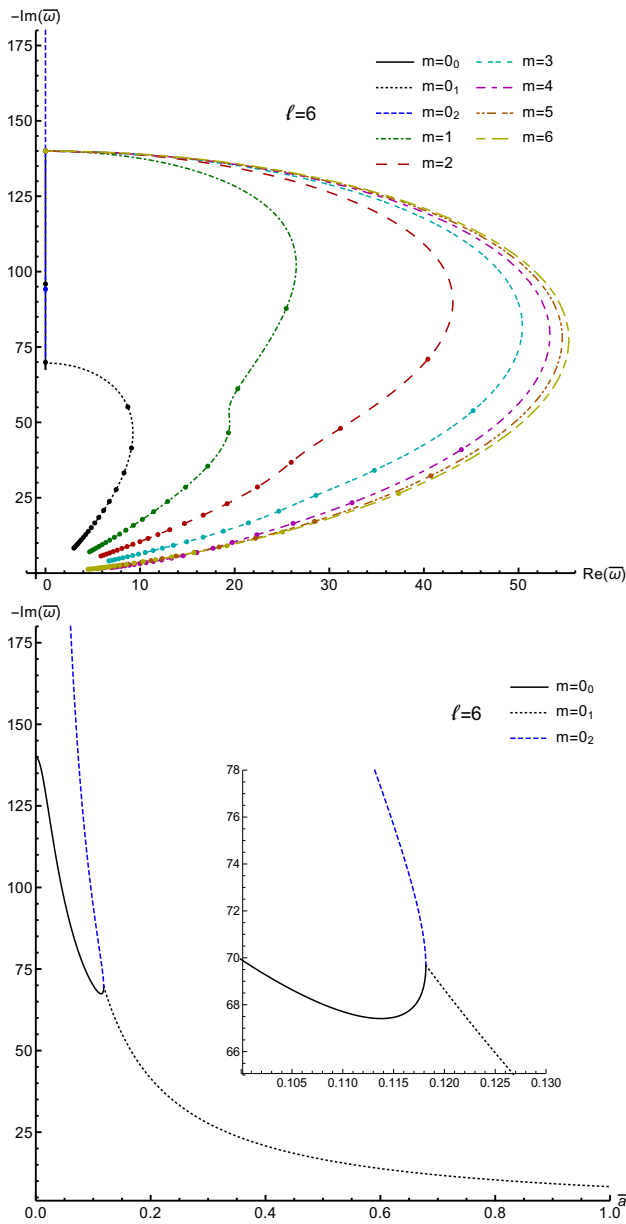


FIG. 6. The TTMs for  $\ell = 6$ . See the caption to Fig. 3 for details.

#### IV. ASYMPTOTIC BEHAVIOR OF THE $m = 0$ MODES

We will refer to the  $m = 0_2$  branch of a given  $m = 0$  TTM sequence as the *asymptotic* branch because we find that  $\lim_{\bar{a} \rightarrow 0} \bar{\omega}(\bar{a}) = -i\infty$  and because it involves the asymptotic behavior of the separation constant  ${}_s A_{\ell m}(\bar{a}\bar{\omega})$ . As mentioned above, to our knowledge, this asymptotic branch had gone unnoticed prior to the work of Ref.[12]. Interestingly, a somewhat similar behavior has recently been noticed in the mode spectrum of rotating black strings[17]. Figure 8 presents a log-log plot of  $\text{Im}(\bar{\omega}(\bar{a}))$  clearly showing the asymptotic behavior of the  $m = 0_0$  branches. The asymptotic branches

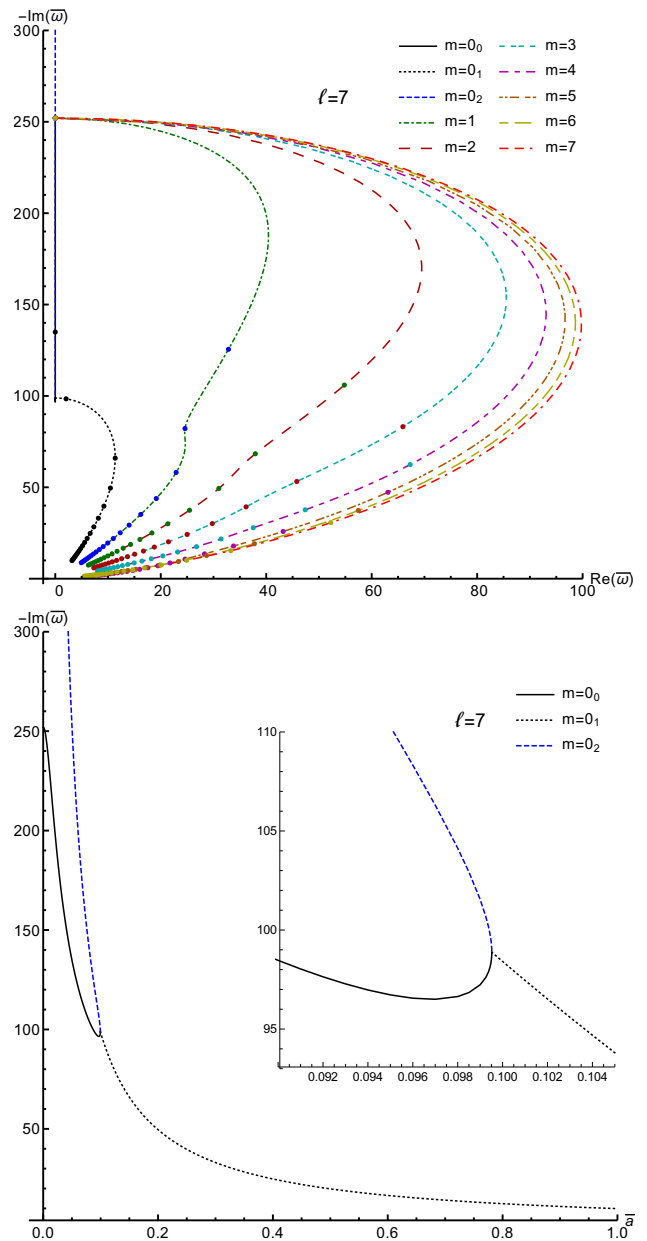


FIG. 7. The TTMs for  $\ell = 7$ . See the caption to Fig. 3 for details.

have power-law behavior and appear to be independent of  $\ell$  at leading order.

Simple fitting of the slope shows that the leading order asymptotic behavior is  $\bar{\omega} \propto a^{-4/3}$ . We could also fit for the proportionality constant, but we can do better by making use of the magnitude squared of the Starobinsky constant  $|Q|^2$  as given in Eq. (6). However, to proceed along this path, we also need to know the asymptotic behavior of the separation constant  ${}_s A_{\ell m}(\bar{a}\bar{\omega})$ .

For mode frequencies on the NIA, the oblateness parameter  $c = a\omega = \bar{a}\bar{\omega}$  of the angular Teukolsky equation, Eq. (4), is purely imaginary. In a more general context, the angular Teukolsky equation is the equation for the

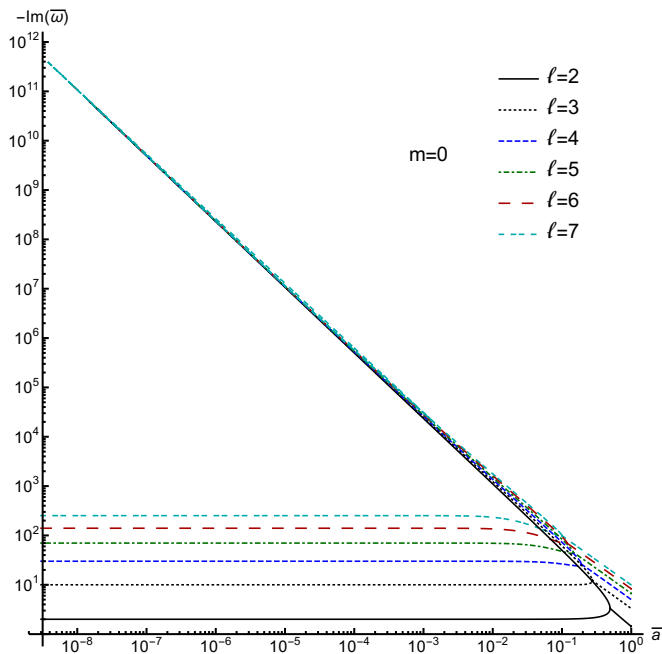


FIG. 8. log–log plot of  $\bar{\omega}$  for  $m = 0$  and  $\ell = 2-7$ , clearly showing the asymptotic behavior of the  $m = 0_2$  branches.

spin-weighted spheroidal function defining the  $x = \cos\theta$  angular dependence of the spin-weighted spheroidal harmonics (SWSHs). For spin-weight  $s = 0$ , the SWSHs are the spheroidal harmonics where real values for the oblateness parameter  $c$  correspond to an *oblate* spheroidal geometry, while imaginary values of  $c$  correspond to *prolate* spheroidal geometry. This terminology extends to the SWSHs. While general solutions for SWSHs and their associated eigenvalues  ${}_s A_{\ell m}(c)$  must be determined numerically, quite a bit is known about them in certain limits[18]. Unfortunately, for the asymptotic prolate case relevant to us, relatively little is known. For general values of  $\ell$ ,  $m$ , and  $s$ , the asymptotic value of  ${}_s A_{\ell m}(c)$  is known only to leading order in  $c$ , and takes the form[18]

$${}_s A_{\ell m}(c) = (2L + 1)|c| + \mathcal{O}(|c|^0), \quad |c| \rightarrow \infty, \quad (12)$$

where

$$L = \ell - \max(|m|, |s|). \quad (13)$$

Fortunately, the known leading order asymptotic behavior of the separation constant in the prolate case is sufficient to allow us to determine the asymptotic behavior of the  $\bar{\omega}$ . If we take  $\bar{\omega} \rightarrow -iC_1 a^{-4/3}$  and  ${}_s A_{\ell 0}(\bar{a}\bar{\omega}) \rightarrow (2L + 1)C_1 a^{-1/3}$  in Eq. (6), and make a power series expansion in powers of  $a$ , we find that the vanishing of  $|\mathcal{Q}|^2$  yields

$$C_1^2 \frac{C_1^6 - 144}{a^{8/3}} - 4C_1^7 \frac{2L + 1}{a^{7/3}} + \mathcal{O}(a^{-7/3}) = 0. \quad (14)$$

We emphasize that this expression is obtained for both  $s = \pm 2$ . The vanishing of the leading-order coefficient

yields  $C_1 = 12^{1/3}$ , independent of  $\ell$  as expected from Fig. 8. The coefficient of the next term depends on  $\ell$ , through  $L$  from the leading order behavior of  ${}_s A_{\ell 0}(c)$ . Vanishing of the coefficient of the second term depends on higher order behavior of  $\bar{\omega}$ . For this term to contribute at  $\mathcal{O}(\bar{a}^{-7/3})$  in  $|\mathcal{Q}|^2$ , the next term in the expansion of  $\bar{\omega}$  must be  $\mathcal{O}(\bar{a}^{-1})$ . If we repeat the procedure above with  $\bar{\omega} \rightarrow -i(C_1 \bar{a}^{-4/3} + C_2 \bar{a}^{-1})$ , we find that the vanishing of  $|\mathcal{Q}|^2$  yields

$$C_1^2 \frac{C_1^6 - 144}{\bar{a}^{8/3}} - 4C_1 \frac{C_1^6(2L + 1) + C_2(72 - 2C_1^6)}{\bar{a}^{7/3}} + \mathcal{O}(\bar{a}^{-2}) = 0. \quad (15)$$

Again, this expression is obtained for both  $s = \pm 2$ . The second term allows us to determine

$$C_2 = (2L + 1) \frac{C_1^6}{2C_1^2 - 72}. \quad (16)$$

Thus, by using  $|\mathcal{Q}|^2 = 0$ , knowing only the leading order term in the asymptotic expansion for  ${}_s A_{\ell m}(c)$ , and assuming the leading order asymptotic falloff is  $\bar{a}^{-4/3}$ , we can determine the first two terms of the asymptotic expansion for  $\bar{\omega}$  to be

$$\bar{\omega}(\bar{a}) = -i \left( \frac{12^{1/3}}{\bar{a}^{4/3}} + \frac{2(2\ell - 3)}{3\bar{a}} \right) + \mathcal{O}(\bar{a}^{-2/3}), \quad (17)$$

and we have chosen to write this expression in terms of  $\ell$ , instead of  $L$ , because it is only valid for  $m = 0$  and  $s = \pm 2$ .

To extend this expansion for  $\bar{\omega}$  further by this method requires that we know the asymptotic form for  ${}_s A_{\ell m}(c)$  to higher order. While this is not known analytically, we can fit our TTM sequences to determine the unknown terms. We will use general expansions of the following forms

$$\bar{\omega} = -i \left[ \frac{C_1}{\bar{a}^{4/3}} + \frac{C_2}{\bar{a}} + \frac{C_{\pm 3}}{\bar{a}^{2/3}} + \frac{C_4}{\bar{a}^{1/3}} + C_5 + C_6 \bar{a}^{1/3} + \dots \right], \quad (18)$$

$${}_{\pm 2} A_{\ell 0}(c) = (2L + 1)|c| + A_{\pm 1} + \frac{A_2}{|c|} + \frac{A_3}{|c|^2} + \frac{A_4}{|c|^3} + \dots \quad (19)$$

The need for the  $\pm$  notation on  $C_{\pm 3}$  and  $A_{\pm 1}$  will be explained in detail below. The coefficients  $C_1$  and  $C_2$  have already been fixed by the vanishing of the first two terms in the power series expansion of  $|\mathcal{Q}|^2 = 0$ . The third term, after replacing  $C_1$  and  $C_2$  yields, for  $s = 2$

$$C_{+3} = \frac{4L(L + 1) - 29 + 6A_{+1}}{9 \times 12^{1/3}}, \quad (20)$$

and for  $s = -2$

$$C_{-3} = \frac{4L(L + 1) - 53 + 6A_{-1}}{9 \times 12^{1/3}}. \quad (21)$$

So, the  $C_{\pm 3}$  coefficients can be determined once the  $A_{\pm 1}$  coefficients are known.

We can find the  $A_{\pm 1}$  coefficient numerically in 2 independent ways. First, we can fit our numerical data for  $\bar{\omega}(\bar{a})$  against Eq. (18). With known values for  $C_1$  and  $C_2$ , and using Eqs. (20) and (21), we can use least-squares fitting to extract numerical values for  $A_{\pm 1}$  from our data for  $\bar{\omega}(\bar{a})$  for  $2 \leq \ell \leq 7$ . We can then find fitting functions for the extracted values of  $A_{\pm 1}(\ell)$ . From the  $A_{+1}$  data ( $s = 2$ ) we find

$$A_{+1} = - \left( \frac{1}{2}L(L+1) - \frac{5}{4} \right). \quad (22)$$

From the  $A_{-1}$  data ( $s = -2$ ) we find

$$A_{-1} = - \left( \frac{1}{2}L(L+1) - \frac{21}{4} \right). \quad (23)$$

Inserting these into Eqs. (20) and (21), we find the shared result

$$C_{\pm 3} = \frac{2L(L+1) - 43}{18 \times 12^{1/3}}. \quad (24)$$

Even though the  $\text{TTM}_R$  and  $\text{TTM}_L$  modes share the same frequency spectrum, the  $C_{\pm 3}$  and  $A_{\pm 1}$  notation is necessary because  ${}_{-s}A_{\ell m}(c) = {}_sA_{\ell m}(c) + 2s$ . This difference manifests itself only in the constant term in the expansion for  ${}_sA_{\ell m}(c)$ . We can express the  $s$  dependence explicitly in  $A_{\pm 1}$ . Using the additional information from the asymptotic expansion for  ${}_oA_{\ell m}(c)$  (see Ref.[18]), we get

$$A_{\pm 1} = - \left( \frac{1}{2}L(L+1) + \frac{3}{4} - s(s-1) \right). \quad (25)$$

Following a similar procedure, we find we have enough numerical precision to accurately extract the  $A_2$  and  $A_3$  coefficients, allowing us to obtain the values for  $C_4$  and  $C_5$ . Our final result for the asymptotic form for the angular separation constant is

$$\begin{aligned} {}_{\pm 2}A_{\ell 0}(c) &= (2L+1)|c| - \left( \frac{1}{2}L(L+1) + \frac{3}{4} - s(s-1) \right) \\ &\quad - \frac{(2L+1)(L(L+1) + 3 - 16s^2)}{2^4|c|} \\ &\quad - \frac{5(L^4 + 2L^3 + 7L + 3) - 2s^2(91L^2 + 96L - 80)}{2^6|c|^2} \\ &\quad + \mathcal{O}(|c|^{-3}). \end{aligned} \quad (26)$$

We strongly emphasize that, even though this expression is written in a very general way, it is only tested for  $m = 0$  and  $s = \pm 2$  or  $s = 0$ . In particular, the terms involving  $s^2$  could be any even power of  $s$  with an appropriate prefactor. Finally, as the main result from this work, we find that the asymptotic expansion of the  $m = 0$  TTM

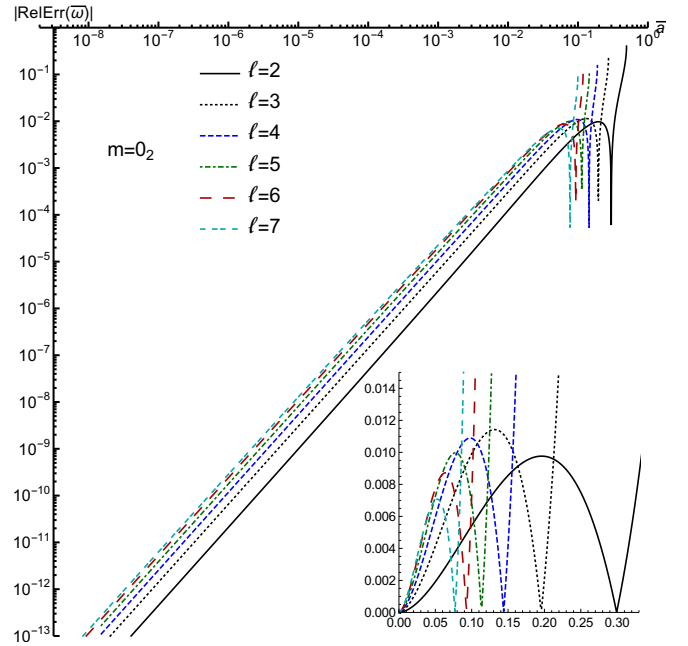


FIG. 9. log-log plot of the relative error in the asymptotic formula for  $\bar{\omega}$  given in Eq. (27). The error is computed relative to the numerical data for  $\bar{\omega}$  for  $m = 0$  and  $\ell = 2-7$ . As expected, the relative error behaves as  $\bar{a}^{5/3}$  in the asymptotic regime. The inset show a standard plot, emphasizing the region where the relative errors are the largest.

frequencies is

$$\begin{aligned} \bar{\omega}(\bar{a}) &= -i \left[ \frac{12^{1/3}}{\bar{a}^{4/3}} + \frac{2(2\ell-3)}{3\bar{a}} + \frac{2\ell^2-6\ell-39}{18 \times 12^{1/3}\bar{a}^{2/3}} \right. \\ &\quad \left. - \frac{(2\ell-3)(19\ell^2-57\ell+2187)}{1296 \times 18^{1/3}\bar{a}^{1/3}} \right. \\ &\quad \left. + \frac{\ell^4-6\ell^3+27\ell-45}{384} \right] \\ &\quad + \mathcal{O}(\bar{a}^{1/3}) \end{aligned} \quad (27)$$

To quantify the accuracy of our expressions for  $\bar{\omega}(\bar{a})$  and  ${}_{\pm 2}A_{\ell 0}(c)$ , we can examine the relative error of these expressions in comparison with our numerical data. Figure 9 shows the relative error in Eq. (27) for  $\bar{\omega}$ . Specifically, we take the difference between Eq. (27) and the numerical data for  $\bar{\omega}$  at the same value of  $\bar{a}$ , and divide this by the value of the numerical data. The absolute value of this quantity is plotted versus  $\bar{a}$ . Clearly, the relative error is quite small in the asymptotic regime where  $\bar{a} \rightarrow 0$ . Since the first unknown term in Eq. (27) goes as  $\bar{a}^{-4/3}$  and the leading order term goes as  $\bar{a}^{-5/3}$ , we expect the relative error to behave as  $\bar{a}^{5/3}$  in the asymptotic regime. This is precisely what is found. Remarkably, Eq. (27) is a very good approximation until reasonably close to the critical value of  $\bar{a}$  at which the  $m = 0_{0,1,2}$  branches meet. Prior to this point on the  $m = 0_2$  branch, we see a “zero crossing” in the relative error for each  $\ell$ , and up until this point, the relative error is always less than 1.2%.

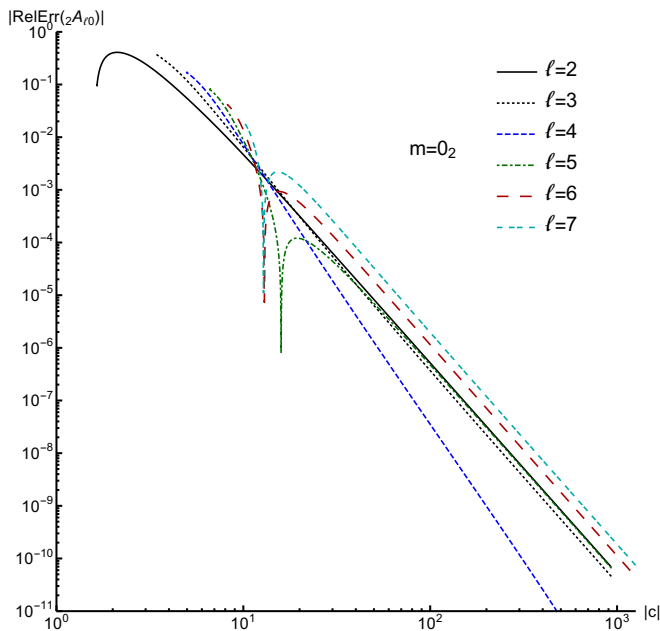


FIG. 10. log–log plot of the relative error in the asymptotic formula for  ${}_2A_{\ell 0}(c)$  given in Eq. (26). The error is computed relative to the numerical data for  ${}_2A_{\ell 0}(c)$  for  $m = 0$  and  $\ell = 2-7$ . As expected, the relative error behaves as  $|c|^{-4}$  in the asymptotic regime.

Figure 10 displays a similar plot showing the relative error in Eq. (26) for  ${}_{\pm 2}A_{\ell 0}(c)$ . Specifically, we take the difference between Eq. (26) and the numerical data for  ${}_2A_{\ell 0}(c)$  at the same value of  $c = \bar{a}\bar{\omega}$ , and divide this by the value of the numerical data. The absolute value of this quantity is plotted versus  $|c|$ , and we remind the reader that  $c$  is purely imaginary. Again, we see that the relative error is quite small in the asymptotic regime where  $|c| \rightarrow \infty$ . Since the first unknown term in Eq. (26) goes as  $|c|^{-3}$  and the leading order term goes as  $|c|$ , we expect the relative error to behave as  $|c|^{-4}$ . This is found for all values of  $\ell$  except for  $\ell = 4$ . In this case the relative error falls off even faster,  $\approx |c|^{-21/5}$ . This is most likely due to the  $\ell = 4$  sequence approaching a “zero crossing” which we see clearly happening for  $\ell = 5-7$ .

## V. SUMMARY AND DISCUSSION

The  $m = 0_0$  and  $0_2$  branches of the various  $m = 0$  TTMs represent very special modes for which the mode frequency is purely imaginary, thus representing modes that are simply decaying with no oscillation. These are the only gravitational modes of the Kerr geometry known to have purely imaginary frequencies, and the  $m = 0_2$  branches were unknown before being noticed in Ref. [12], where the framework to fully understand the behavior of these modes was worked out.

For the most-part, these modes are TTMs with the

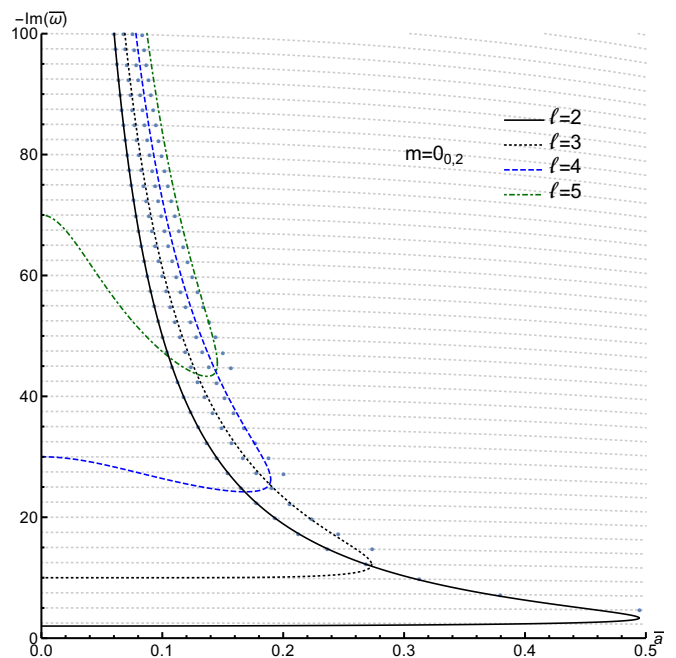


FIG. 11. The locations of non-generic modes are illustrated in this plot.  $\text{Im}(\bar{\omega})$  is plotted as a function of  $\bar{a}$ . The numerical data for the TTMs with  $m = 0_0$  and  $\ell = 2-5$  are plotted as denoted in the figure legend. The  $m = 0_1$  branches, where  $\bar{\omega}$  contains a non-vanishing real component are omitted. The nearly horizontal gray dotted lines show  $\bar{\omega}_+$  as functions of  $\bar{a}$  for the values  $N_+ = 10, 20, 30, \dots$ . The intersection of these gray dotted lines with lines denoting the TTMs are locations where the modes are anomalous. The individual dots denote the estimated location of the anomalous modes based on Eq. (28).

TTM<sub>L</sub>s and the TTM<sub>R</sub>s sharing the same mode frequencies. However, for each  $\ell$ , there are a countably-infinite number of frequencies where the modes are either “anomalous” or “miraculous” in the language of Ref. [12]. At these special frequencies, the modes that would normally be just TTM<sub>L</sub>s are also simultaneously QNMs. Furthermore the modes that would normally be just TTM<sub>R</sub>s are neither TTMs nor QNMs.

This non-generic behavior occurs when the roots of the indicial equation differ by an integer for the Frobenius solution local to the event horizon. The condition for this is

$$\bar{\omega} = \bar{\omega}_+ \equiv \frac{\bar{a}m - iN_+\sqrt{1-\bar{a}^2}}{2(1+\sqrt{1-\bar{a}^2})}, \quad (28)$$

where  $N_+$  is an integer when  $s$  is an integer, and it is a half-odd integer when  $s$  is a half-odd integer. Two possible non-generic behaviors can occur. In the simplest case, only one series solution can exist, and it corresponds to the local Frobenius solution with the largest exponent. The second solution will include a logarithmic term. This is the *anomalous* case. In certain circumstances, the coefficient multiplying the logarithmic term can vanish. This is the *miraculous* case.

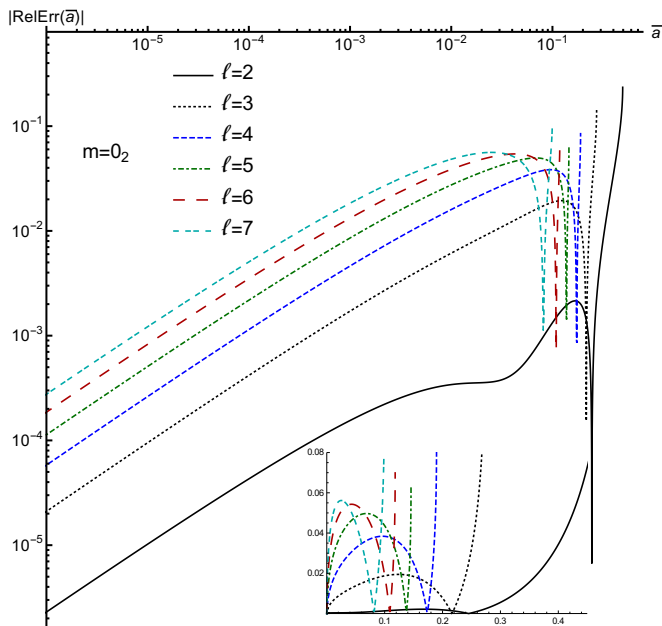


FIG. 12. log-log plot of the relative error in the estimated value of  $\bar{a}$  for the non-generic modes as a function of  $\bar{a}$ . The inset shows a standard plot, emphasizing the region where the errors are the largest.

For gravitational modes of Kerr, when  $s = -2$ , the  $m = 0_0$  and  $0_2$  branches are normally  $\text{TMM}_{\text{L}}$ s. But when the mode frequencies satisfy Eq. (28) for some integer value of  $N_+$ , then the solutions are *anomalous*. The outgoing mode in this case has exactly the same local

behavior as the incoming mode.<sup>3</sup> Therefore, the  $s = -2$  modes with frequencies satisfying Eq. (28) are simultaneously  $\text{TMM}_{\text{L}}$ s and QNMs. But, for the  $s = +2$  modes which are normally  $\text{TMM}_{\text{R}}$ s, when the mode frequencies satisfy Eq. (28) for some integer value of  $N_+$ , then the solutions are *miraculous*. In this case, the behavior local to the event horizon is a linear combination of incoming and outgoing modes, violating the conditions for the modes to be  $\text{TMM}_{\text{R}}$ s.

The locations where these non-generic modes occur is illustrated in Fig. 11. For clarity, only the  $m = 0_0$  and  $0_2$  mode sequences for  $\ell = 2-5$  from the numerical data are included. In addition,  $\omega_+$  from Eq. (28) is plotted as a function of  $\bar{a}$ . Each nearly horizontal dotted-gray line represents a specific value of  $N_+$ . Again for clarity, only the values of  $N_+ = 10, 20, 30, \dots$  are plotted. Non-generic modes occur whenever the dotted-gray lines cross one of the sequences of numerical modes.<sup>4</sup> We emphasize that only 1 in 10 of the crossing is actually shown in Fig. 11.

We can find the approximate value of  $\bar{a}$  for each of the crossings of the  $m = 0_2$  branches by equating Eqs. (27) and (28). To leading order, we find  $\bar{a}_+ \approx 4 \cdot 3^{1/4} N^{-3/4}$ . This is independent of  $\ell$ , and while it gives a good approximation to  $\bar{\omega}$  at each crossing, it is not a good approximation for the value of  $\bar{a}$  itself.

If we include all the terms in Eq. (27), but only the leading order term in the expansion of Eq. (28), then we have a system that is consistent to  $\mathcal{O}(\bar{a}^{1/3})$ . If we take  $\bar{a}_+ = 4 \cdot 3^{1/4} N^{-3/4} (1 + \alpha)$  and assume  $\alpha$  is small, expanding to linear order in  $\alpha$  finally yields

$$\bar{a}_+ \approx \frac{3456 \cdot 3^{1/4} N_+^{1/2} + 1152(2\ell - 3)N_+^{1/4} - 16 \cdot 3^{3/4}(14\ell^2 - 42\ell + 75)}{864 N_+^{5/4} - 48 \cdot 3^{3/4}(2\ell - 3)N_+ + 8 \cdot 3^{1/2}(14\ell^2 - 42\ell + 75)N_+^{3/4} - 9 \cdot 3^{1/4}(2\ell - 3)(7\ell^2 - 21\ell - 25)N_+^{1/2}}. \quad (29)$$

In Fig. 11, the small dots represent the approximation for the location of the crossings using Eqs. (29) and (28). The approximation is clearly excellent for  $\ell = 2$ , with increasing error as  $\ell$  increases. Figure 12 displays the relative error of the approximate location of the crossings. It is obtained by treating  $N_+$  as a continuum variable and obtaining its value for each point in the numerical data along the asymptotic branches. Using  $\ell$ ,  $\bar{a}$ , and the so-obtained value of  $N_+$  from each numerical sequence, we can compute the error relative to the actual value of  $\bar{a}$ .

In this way, Fig. 12 shows the relative error inherent in Eq. (29).

These asymptotic modes are intriguing, and while we have been able to elucidate their properties with significant precision, their physical importance is less clear. All of the modes of concern have frequencies that lie on the NIA, and are restricted to  $m = 0$ . Because the frequencies are purely imaginary, the individual modes represent pure damping states. Furthermore, these are all highly damped states. For comparison, the fastest damping fundamental  $\ell = 2$  QNM is more than 20 times smaller than the slowest damping mode on the NIA with  $\bar{\omega} = -2i$ .

The  $s = -2$  gravitational modes with frequencies on the NIA are all  $\text{TMM}_{\text{L}}$ s, but at certain values of  $\bar{a}$ , they are also simultaneously QNMs. At these same values of  $\bar{a}$ , the  $s = 2$   $\text{TMM}_{\text{R}}$ s with modes frequencies on the NIA do not satisfy the boundary conditions for  $\text{TMM}_{\text{R}}$ s.

<sup>3</sup> This is due to strong scattering of the outgoing mode off of the potential tail. The scattering is so strong that it overwhelms the normally dominant behavior of the outgoing mode. See Sec. IV.D of Ref. [12] for details.

<sup>4</sup> These crossings are precisely what was plotted as black dots in Fig. 20 of Ref. [12].

Given this behavior, we are tempted to think of the set of modes which are simultaneously  $\text{TTM}_L$  and QNM as somehow, in the asymptotic limit, hinting at a discreteness in the allowed values of  $\bar{a}$ . Certainly, there is a “correspondence principle” like behavior as  $\bar{a} \rightarrow 0$  where the spacing between adjacent values of  $\bar{a}$  becomes vanishingly small with  $\Delta\bar{a} \sim \bar{a}^{7/3}$ .

However, our consideration of this very regular behavior in these particular modes on the NIA is ignoring another set of QNMs that exist on the NIA and satisfy  $\bar{\omega}_- = -iN_-/4$  (see Ref.[12]). These modes do not exist for all allowed values of  $N_-$ , and the determination of the value of  $\bar{a}$  at which these QNM do exist is less easily

analyzed. Furthermore, these special modes that are simultaneously QNM and  $\text{TTM}_L$  are not isolated modes but rather represent termination points of sequences of modes that otherwise do not have frequencies on the NIA.

In conclusion, we cannot yet say if these modes carry any important physical significance. Never-the-less, they are present in the QNM/TTM spectrum.

## ACKNOWLEDGMENTS

Some computations were performed on the Wake Forest University DEAC Cluster, a centrally managed resource with support provided in part by the University.

- 
- [1] R. P. Kerr, Phys. Rev. Lett. **11**, 237 (1963).
  - [2] B. P. Abbott *et al.* (LIGO Scientific Collaboration and Virgo Collaboration), Phys. Rev. Lett. **116**, 061102 (2016).
  - [3] B. P. Abbott *et al.* (LIGO Scientific Collaboration and Virgo Collaboration), Phys. Rev. Lett. **116**, 241103 (2016).
  - [4] B. P. Abbott *et al.* (LIGO Scientific Collaboration and Virgo Collaboration), Phys. Rev. Lett. **118**, 221101 (2017).
  - [5] B. P. Abbott *et al.* (LIGO Scientific Collaboration and Virgo Collaboration), Phys. Rev. Lett. **119**, 141101 (2017).
  - [6] R. M. Wald, J. Math. Phys. (N.Y.) **14**, 1453 (1973).
  - [7] S. Chandrasekhar, Proc. R. Soc. A **392**, 1 (1984).
  - [8] H. Onozawa, Phys. Rev. D **55**, 3593 (1997).
  - [9] G. B. Cook and M. Zalutskiy, Phys. Rev. D **90**, 124021 (2014).
  - [10] E. W. Leaver, Proc. R. Soc. A **402**, 285 (1985).
  - [11] A. Maassen van den Brink, Phys. Rev. D **62**, 064009 (2000).
  - [12] G. B. Cook and M. Zalutskiy, Phys. Rev. D **94**, 104074 (2016).
  - [13] G. B. Cook and M. Zalutskiy, Classical Quantum Gravity **33**, 245008 (2016).
  - [14] A. Ronveaux, ed., *Heun's Differential Equations* (Oxford University, New York, 1995).
  - [15] R. S. Borissov and P. P. Fiziev, Bulg. J. Phys. **37**, 65 (2010).
  - [16] E. Berti, V. Cardoso, and C. M. Will, Phys. Rev. D **73**, 064030 (2006).
  - [17] L. A. H. Mamani, J. Morgan, A. S. Miranda, and V. T. Zanchin, Phys. Rev. D **98**, 026006 (2018).
  - [18] E. Berti, V. Cardoso, and M. Casals, Phys. Rev. D **73**, 024013 (2006).